ETH
Eidgenössische Technische Hochschule Zürich
Swiss Federal Institute of Technology Zurich

Seminar for Applied Mathematics SAM

Anderson localization in the subwavelength regime

H. Ammari and B. Davies and E.O. Hiltunen

Research Report No. 2022-23
May 2022

Seminar für Angewandte Mathematik
Eidgenössische Technische Hochschule
CH-8092 Zürich
Switzerland

Funding SNF: 200021--200307

Anderson localization in the subwavelength regime

Habib Ammari* Bryn Davies† Erik Orvehed Hiltunen‡

Abstract

Random media are ubiquitous in both natural and artificial structures and there are many important problems related to understanding their wave-scattering properties. In particular, the phenomenon of wave localization in random media, known as Anderson localization in certain settings, has proved difficult to understand, particularly in physically derived models and systems with long-range interactions. In this article, we show that the scattering of time-harmonic waves by high-contrast resonators with randomly chosen material parameters reproduces the characteristic features of Anderson localization and its properties can be understood using our asymptotic results. In particular, we show that the hybridization of subwavelength resonant modes is responsible for both the repulsion of energy levels as well as the widely observed phase transition, at which point eigenmode symmetries swap and very strong localization is possible. We derive results from first principles, using asymptotic expansions in terms of the material contrast parameter, and obtain a characterisation of the localized modes in terms of Laurent operators and generalized capacitance matrices. This model captures the long-range interactions of the wave-scattering system and provides a rigorous framework to explain the exotic phenomena that are observed.

Mathematics Subject Classification (MSC2010): 35J05, 35C20, 35P20, 78A48.

Keywords: disordered systems, subwavelength resonance, phase transition, level repulsion, high-contrast metamaterials, asymptotic analysis.

1 Introduction

As waves propagate through our environment they often encounter randomly perturbed materials. These random media might be organic substances, fluids or structured materials that have been subjected to random perturbations. As a result, there is a large field concerned with the propagation of waves in random media [16, 20]. One eye-catching phenomenon is the localization of waves in random media. The seminal work in this area was the observation by Philip Anderson in 1958 that random media could be free from diffusion [9]. His work concerned the transport of electrons in random lattices, but has inspired studies in many different wave regimes [10, 12, 13, 15, 22, 26, 28].

Wave localization is typically constrained by the diffraction limit. In the case of Anderson localization, the localization length is typically limited by the wavelength and diverges in the low-frequency regime. In this classical setting, inhomogeneities on length-scales smaller than the wavelength will have a negligible effect on wave scattering, and wave transport is characterized by effective parameters where any small disorder is averaged. However, recent developments of *subwavelength* wave localization are able to overcome this barrier [2, 19, 27]. Crucially, this is achieved in *locally resonant* materials, whose constituents exhibit resonance at small (*i.e.*, *subwavelength*) frequencies. In particular, *high-contrast* resonators are a natural example of subwavelength resonance (see *e.g.* [2] for a comprehensive review of related phenomena; a famous example is the Minnaert resonance of air bubbles in water [24]). A periodic crystal of N repeated resonators is known to have N subwavelength resonant band functions. A band gap is guaranteed to exist above these bands and possibly between them, depending on the choice of geometry [2]. Compact perturbations can create eigenmodes with eigenfrequencies within these band gaps. These 'midgap' modes are elements of the point spectrum and cannot couple with

*Department of Mathematics, ETH Zurich, Zurich, Switzerland (habib.ammari@math.ethz.ch).
†Department of Mathematics, Imperial College London, London, UK (bryn.davies@imperial.ac.uk).
‡Department of Mathematics, Yale University, New Haven, USA (erik.hiltunen@yale.edu).

the Bloch modes so decay exponentially quickly away from the defect. Some examples of localized modes, for a planar square lattice of high-contrast three-dimensional resonators are shown in Figure 1. We can derive explicit formulas of the the midgap frequencies and can describe the localized modes of a fully random structure by increasing the number of perturbations.

The behaviour of the randomly perturbed systems studied here can be understood by considering the simple phenomena of *hybridization* and *level repulsion*. That is, when two eigenmodes are coupled, one of the eigenfrequencies of the resulting hybridized modes will be shifted up while the other will be shifted down. Meanwhile, level repulsion describes the observation that when disorder is added to the entries of a matrix, the eigenvalues have a tendency to separate [23]. These can be used to explain, firstly, the observation that the stronger the disorder, the more localized modes are created, as well as the tendency for the eigenmodes to become more strongly localized as the strength of the disorder increases. The most commonly studied random matrices are Gaussian ensembles, for which the distributions of eigenvalue separations are well known [23]. In our setting, however, we have a non-linear eigenvalue problem so are not able to use this theory. As a result, we will elect to study uniformly distributed perturbations. However, in many cases we noticed very similar results for Gaussian perturbations.

The phase transition whereby disordered media changes from being conducting (exhibiting only weak localization) to being insulating (the absence of diffusion) is sometimes referred to as the *Anderson transition* [22]. In this work, we similarly observe a phase transition at a positive value of the perturbation strength. At this transition, eigenfrequencies become degenerate and the symmetries of the corresponding modes swap (*i.e.* monopole modes change to dipole modes, and conversely). In general, when eigenmodes hybridize, the volume of their support increases, decreasing the extent to which they can be said to be localized. This can, however, be mitigated at the phase transition. At this point, any small perturbation will lift the degeneracy and cause the modes to decouple, producing strongly localized modes. A sharp peak in the average degree of localization is observed here, which is the key signature of the transition.

The analysis in this work is based on the *generalized capacitance matrix*, which is a powerful tool for characterising the subwavelength resonant modes of a system of high-contrast resonators [2]. In essence, the capacitance formulation provides a discrete approximation to the continuous spectral problem of the PDE-model, valid asymptotically in terms of the high contrast. This approximation is based solely on first principles, and provides a natural starting point for analysis and numerical simulation of Anderson localization. The inclusion of *long-range interactions* is a crucial feature of the capacitance matrix: the off-diagonal entries C_{ij} decay slowly, according to $1/|i-j|$. In contrast, previous studies of Anderson localization are mainly limited to the case of short-range interactions $1/|i-j|^{d+\varepsilon}$, where d is the dimension and $\varepsilon > 0$ [1, 9, 14]. Since Anderson's original work [9], localization was believed to only occur in systems with short-range interactions but, more recently, localization has been demonstrated in systems with long-range interactions [21, 25].

Although Anderson localization has been studied in systems related to the current setting, most notably for classical waves in [14], the analysis is typically based on approximating the continuous (differential) equation by a discrete (difference) equation. In contrast, the discrete capacitance approximation studied in this work is derived from first principles and is a natural approximation based on the physical properties of the system. It is important to emphasize that tight-binding formulations are not applicable in the setting of high-contrast resonators [5, 17, 18].

The analysis in this work deepens the understanding of localization in systems with long-range interactions. We begin by describing the Helmholtz PDE-model of interest in Section 2, and derive the corresponding generalized capacitance formulation in Section 3. The Helmholtz problem is now approximated by a spectral problem for a Laurent operator, where the random disorder is manifested through multiplication of a diagonal operator. The capacitance formulation also allows a fully explicit characterization of localized modes in the case of finite defects, whereby the problem reduces to a nonlinear eigenvalue problem for a Toeplitz matrix. Before studying the fully random case, we consider a simpler case with only finitely many perturbations in Section 4. This allows for a detailed study of level repulsion and phase transition, providing insight into the mechanism of Anderson localization in systems with long-range interations. Due to the phenomenon of level repulsion, these perturbations will induce frequencies inside the band gap corresponding to localized modes and will do so in a way that is robust to imperfections. The random perturbations serve to decouple the midgap modes, resulting in a high degree of localization. At the phase transition point, strong localization is achievable

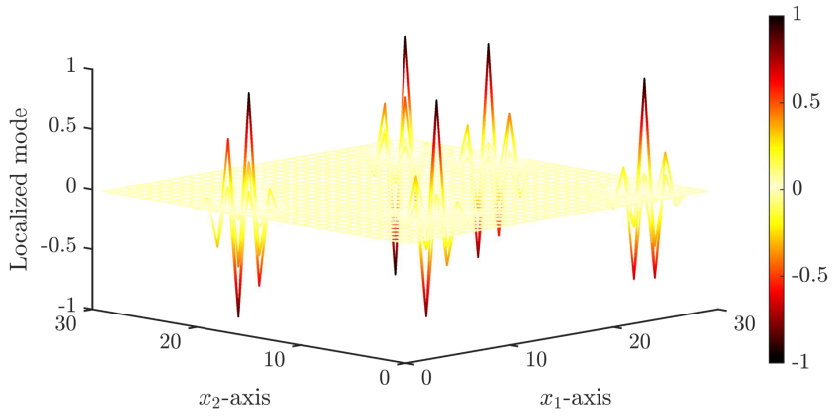

Figure 1: Examples of localized states in a two-dimensional, finite, square lattice. Here shown in the case of $N = 900$ resonators and random perturbations drawn from a uniform distribution with standard deviation $\sigma = 0.05$; see Section 5 for details of the setup.

with an exceptionally small random perturbation. Additionally, we study the limit when the number of defects increases, demonstrating an increasing number of localized modes. Finally, in Section 5 we consider the fully random case, *i.e.*, when *all* resonators are taken to have random parameters. As observed in discrete systems with short-range interactions (see, *e.g.*, [14]), the band structure of the unperturbed case persists, while localized modes emerge around the edges of the bands. As the perturbation increases, the level repulsion will cause the localized frequencies to separate and increase the degree of localization.

2 Formulation of the resonance problem

We assume that the resonator system consists of periodically arranged scatterers, whose material parameters may be non-periodic. We work in d spatial dimensions and take a lattice Λ of dimension $d_l \leq d$, generated by the lattice vectors $l_1, ..., l_{d_l}$:

$$\Lambda := \{m_1 l_1 + ... + m_{d_l} l_{d_l} \mid m_i \in \mathbb{Z}\}.$$

We let $P_l : \mathbb{R}^d \to \mathbb{R}^{d_l}$ be the projection onto the first d_l coordinates, and $P_\perp : \mathbb{R}^d \to \mathbb{R}^{d-d_l}$ be the projection onto the last $d - d_l$ coordinates. For simplicity, we assume that $P_\perp l_i = 0$, which means that the lattice is aligned with the first d_l coordinate axes. For a point $x \in \mathbb{R}^d$, we use the notation $x = (x_l, x_0)$, where $x_l = P_l x$ and $x_0 P_\perp x$. We let $Y \subset \mathbb{R}^d$ be a fundamental domain of the given lattice:

$$Y := \{c_1 l_1 + ... + c_{d_l} l_{d_l} \mid 0 \leq c_1, ..., c_{d_l} \leq 1\}.$$

Inside Y, we assume that there are N scatterers, or *resonators*, $D_i \subset Y$, for $i = 1, ..., N$. These are disjoint, connected domains with boundaries in $C^{1,s}$ for some $0 < s < 1$. For $m \in \Lambda$, we let D_i^m denote the translated resonator, and we let $\mathcal{D}$ denote the total collection of resonators:

$$\mathcal{D} = \bigcup_{m \in \Lambda} \bigcup_{i \in \{1,...,N\}} D_i^m, \qquad D_i^m = D_i + m.$$

We let v_i^m denote the wave speed in D_i^m, and v denote the wave speed in the surrounding medium. Each resonator is additionally associated to a parameter δ_i^m, which describes the contrast between the resonator and the surrounding. The natural setting to achieve subwavelength resonance is to consider the *high-contrast* case [2], whereby we assume that

$$\delta_i^m = O(\delta)$$

for some small parameter $\delta \to 0$.

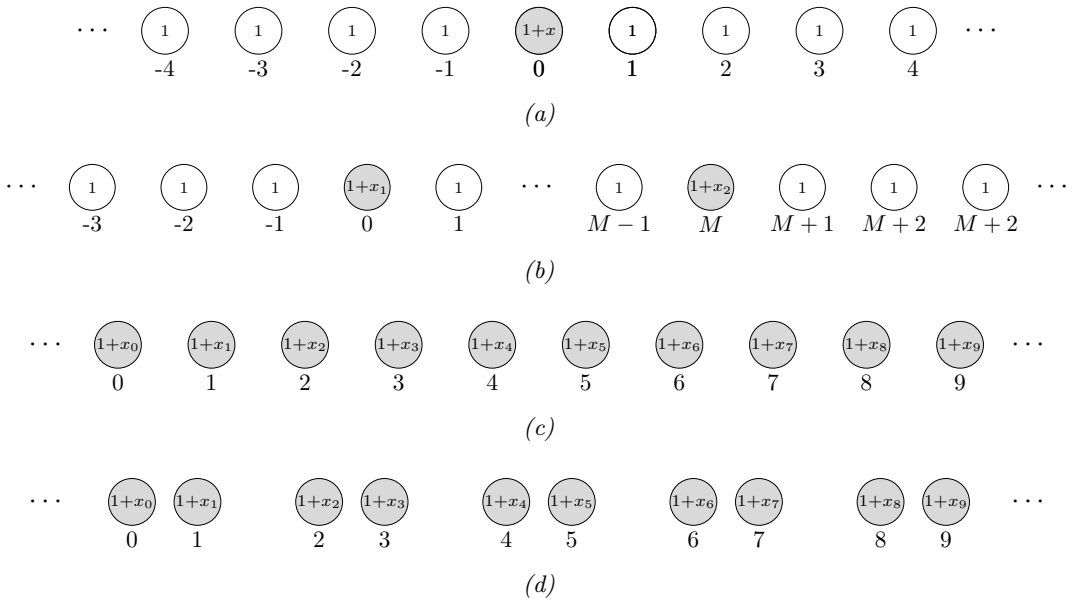

Figure 2: Arrays of resonators with (a) a single defect, on the 0^{th} resonator, (b) two defects, on the 0^{th} and the M^{th} resonators, (c) defects on every resonator, and (d) defects on every resonator in an array of dimers. In each case, the material parameters on defective resonators are perturbed $1 \mapsto 1+x_i$ for some $x_i \in (-1, \infty)$. We depict circular resonators here, but the theoretical results in this work hold for any shape with Hölder continuous boundary. In this work, we conduct analytic studies of structures (a) and (b) to make predictions about the behaviour of (c) and (d).

Throughout this work, we will consider the equation

$$\begin{cases} \Delta u + \dfrac{\omega^2}{v^2} u = 0 & \text{in } \mathbb{R}^d \setminus \mathcal{D}, \\ \Delta u + \dfrac{\omega^2}{(v_i^m)^2} u = 0 & \text{in } D_i^m,\ i = 1, \dots, N, \\ u|_+ - u|_- = 0 & \text{on } \partial\mathcal{D}, \\ \delta_i^m \dfrac{\partial u}{\partial \nu}\Big|_+ - \dfrac{\partial u}{\partial \nu}\Big|_- = 0 & \text{on } \partial D_i^m,\ i = 1, \dots, N, \\ u(x_l, x_0) & \text{satisfies the outgoing radiation condition as } |x_0| \to \infty. \end{cases} \tag{2.1}$$

The dual lattice of Λ, denoted Λ^*, is generated by $\alpha_1, ..., \alpha_{d_l}$ satisfying $\alpha_i \cdot l_j = 2\pi\delta_{ij}$ and $P_\perp \alpha_i = 0$, for $i, j = 1, ..., d_l$. The *Brillouin zone* Y^* is defined as $Y^* := \left(\mathbb{R}^{d_l} \times \{\mathbf{0}\}\right)/\Lambda^*$, where $\mathbf{0}$ is the zero-vector in $\mathbb{R}^{d-d_l}$. We remark that Y^* can be written as $Y^* = Y_l^* \times \{\mathbf{0}\}$, where Y_l^* has the topology of a torus in d_l dimensions.

3 Generalized capacitance matrices and Laurent operators

In this section, we introduce the capacitance matrix formalism, which characterizes the subwavelength spectrum of (2.1) in terms of a discrete Laurent operator. In its simplest form, the generalized quasiperiodic capacitance matrix $\mathcal{C}^\alpha$, gives a concise characterization of the periodic problem. We then generalize this framework to a general, possibly random, parameter distribution. Similar characterisations, in terms of the generalized capacitance matrix, have been used to study the subwavelength resonant modes of many different systems of high-contrast resonators, see [2] for a review. In the case of a compact perturbation of a periodic system, this Laurent-operator formalism reduces to an eigenvalue problem for a Toeplitz matrix.

3.1 Layer potentials and the generalized capacitance matrix

In the case of a periodic system, the spectrum of (2.1) is well-understood (see, for example, [2]). In this section, we briefly summarize the main results. We assume that the material parameters satisfy

$$\delta_i^m = \delta_i, \qquad v_i^m = v_i, \qquad \text{for all } m \in \Lambda,$$

for some constants δ_i, v_i, $i = 1, ..., N$.

In the case $\alpha \notin Y \setminus \{0\}$, we can define the quasiperiodic Green's function $G^\alpha(x)$ as the Floquet transform of $G^k(x)$ in the first d_l coordinate dimensions, *i.e.*,

$$G^\alpha(x) := \sum_{m \in \Lambda} G(x - m) e^{\mathrm{i}\alpha \cdot m}. \tag{3.1}$$

Here G is the Green's function for Laplace's equation in $d = 2$ or $d = 3$. The series in (3.1) converges uniformly for x and y in compact sets of $\mathbb{R}^d$, $x \neq y$ and $\alpha \neq 0$. The quasiperiodic single layer potential $\mathcal{S}_D^\alpha$ is defined as

$$\mathcal{S}_D^\alpha[\varphi](x) := \int_{\partial D} G^\alpha(x - y)\varphi(y)\, \mathrm{d}\sigma(y), \quad x \in \mathbb{R}^d.$$

Definition 3.1 (Quasiperiodic capacitance matrix)**.** Assume $\alpha \neq 0$. For a system of $N \in \mathbb{N}$ resonators $D_1, \ldots, D_N$ in Y we define the quasiperiodic capacitance matrix $C^\alpha = (C_{ij}^\alpha) \in \mathbb{C}^{N \times N}$ to be the square matrix given by

$$C_{ij}^\alpha = -\int_{\partial D_i} (\mathcal{S}_D^\alpha)^{-1}[\chi_{\partial D_j}]\, \mathrm{d}\sigma, \quad i, j = 1, \ldots, N.$$

At $\alpha = 0$, we can define C^0 by the limit of C^α as $\alpha \to 0$ [2].

Definition 3.2 (Generalized quasiperiodic capacitance matrix)**.** For a system of $N \in \mathbb{N}$ resonators $D_1, \ldots, D_N$ in Y we define the generalized quasiperiodic capacitance matrix, denoted by $\mathcal{C}^\alpha = (\mathcal{C}_{ij}^\alpha) \in \mathbb{C}^{N \times N}$, to be the square matrix given by

$$\mathcal{C}_{ij}^\alpha = \frac{\delta_i v_i^2}{|D_i|} C_{ij}^\alpha, \quad i, j = 1, \ldots, N.$$

Since (2.1) is periodic, it is well-known that the spectrum consists of bands parametrized by α. For small δ, there are N such bands $\omega_i(\alpha)$, $i = 1, ..., N$ satisfying $\omega_i(\alpha) = O(\delta^{1/2})$. We have the following result [2].

Theorem 3.3. *Let $d \in \{2, 3\}$ and $0 < d_l \leq d$. Consider a system of N subwavelength resonators in Y, and assume $|\alpha| > c > 0$ for some constant c independent of ω and δ. As $\delta \to 0$, there are N subwavelength resonant frequencies, which satisfy the asymptotic formula*

$$\omega_n^\alpha = \sqrt{\lambda_n^\alpha} + O(\delta^{3/2}), \quad n = 1, \ldots, N.$$

Here, $\{\lambda_n^\alpha : n = 1, \ldots, N\}$ are the eigenvalues of the generalized quasiperiodic capacitance matrix $\mathcal{C}^\alpha \in \mathbb{C}^{N \times N}$, which satisfy $\lambda_n^\alpha = O(\delta)$ as $\delta \to 0$.

3.2 Laurent-operator formulation

The goal, now, is to derive a capacitance formulation which is valid even in the case when the material parameters are not distributed periodically.

Assume that u is a localized eigenmode to (2.1) in the subwavelength regime, *i.e.*, u corresponds to an eigenvalue ω which scales as $O(\delta^{1/2})$. Here, we refer to localization in the L^2-sense and, in addition, we assume that u is normalized, in the sense that

$$\int_{\mathbb{R}^{d_l}} |u(x_l, 0)|^2\, \mathrm{d}x_l = 1 \quad \text{and} \quad \int_{\mathbb{R}^{d_l}} |u(x_l, x_0)|^2\, \mathrm{d}x_l < \infty,$$

for any $x_0 \in \mathbb{R}^{d - d_l}$. We have the following result from [7].

Lemma 3.4. *Let u be a localized, normalized eigenmode to* (2.1) *corresponding to an eigenvalue ω which satisfies $\omega = O(\delta^{1/2})$ as $\delta \to 0$. Then, uniformly in $x \in \mathcal{D}$,*

$$u(x) = u_i^m + O(\delta^{1/2}), \quad x \in D_i^m, i = 1, ..., N, m \in \Lambda,$$

for some u_i^m which are constant with respect to x and δ.

We define $\mathbf{u}^m = \begin{pmatrix} u_1^m \\ \vdots \\ u_N^m \end{pmatrix} \in \mathbb{R}^N$. Since ω is a subwavelength frequency, we can write

$$\omega = \omega_0 + O(\delta), \quad \omega_0 = \beta\delta^{1/2}, \tag{3.2}$$

for some constant β. We denote the material parameters as

$$\delta_i^m (v_i^m)^2 = \delta_i v_i^2 b_i^m$$

for some (possibly random) variables b_i^m which satisfy $b_i^m = O(1)$ as $\delta \to 0$. We define $\mathcal{B}_m$ as the $N \times N$ diagonal matrix whose i^{th} entry is given by b_i^m.

We introduce the Floquet transform $\mathcal{F} : \left(l^2(\Lambda)\right)^N \to \left(L^2(Y^*)\right)^N$ and its inverse $\mathcal{I} : \left(L^2(Y^*)\right)^N \to \left(l^2(\Lambda)\right)^N$, which are given by

$$\mathcal{F}[\phi](\alpha) := \sum_{m\in\Lambda} \phi(m) e^{\mathrm{i}\alpha\cdot m}, \qquad \mathcal{I}[\psi](m) := \frac{1}{|Y^*|}\int_{Y^*} \psi(\alpha) e^{-\mathrm{i}\alpha\cdot m}\, \mathrm{d}\alpha.$$

The Floquet transform is the tool that allows us to show the following result, by transforming into the dual space and then back again.

Proposition 3.5. *Any localized solution u to* (2.1)*, corresponding to a subwavelength frequency $\omega = \omega_0 + O(\delta)$, satisfies*

$$\mathcal{B}_m \sum_{n\in\Lambda} \mathcal{C}^{m-n}\mathbf{u}^n = \omega_0^2 \mathbf{u}^m, \tag{3.3}$$

for every $m \in \Lambda$, where $\mathcal{C}^m = \mathcal{I}[\mathcal{C}^\alpha](m)$.

Proof. From [7] we have that

$$\mathcal{C}^\alpha \sum_{m\in\Lambda} \mathbf{u}^m e^{\mathrm{i}\alpha\cdot m} = \omega_0^2 \sum_{m\in\Lambda} (\mathcal{B}_m)^{-1}\mathbf{u}^m e^{\mathrm{i}\alpha\cdot m}, \tag{3.4}$$

for all $\alpha \in Y^*$. We can choose to pose the problem either in the real (spatial) variable m or in the dual (momentum) variable α. In this framework, equation (3.4), posed in the dual variable α, reads

$$\mathcal{C}^\alpha \mathbf{u}^\alpha = \omega_0^2 \left(\sum_{m\in\Lambda} (\mathcal{B}_m)^{-1} \mathcal{I}[\mathbf{u}^\alpha](m) e^{\mathrm{i}\alpha\cdot m} \right), \qquad \mathbf{u}^\alpha = \mathcal{F}[\mathbf{u}^m](\alpha), \tag{3.5}$$

where we (by abuse of notation) use the same notation for $\mathbf{u}^m$ as its Floquet transform $\mathbf{u}^\alpha$. We can re-frame this equation in the real variable m by taking the inverse Floquet transform. Since $\mathbf{u}^m = \mathcal{I}[\mathbf{u}^\alpha](m)$, we can apply $\mathcal{I}$ to (3.5) to obtain (3.3). □

If we assume that $\Lambda = \mathbb{Z}$, the system of equations (3.3) is easier to visualize. In this case, we can introduce the doubly infinite matrices and vectors

$$\mathfrak{C} = \begin{pmatrix} \ddots & \vdots & \vdots & \vdots & \vdots & \iddots \\ \cdots & \mathcal{C}^0 & \mathcal{C}^1 & \mathcal{C}^2 & \mathcal{C}^3 & \cdots \\ \cdots & \mathcal{C}^{-1} & \mathcal{C}^0 & \mathcal{C}^1 & \mathcal{C}^2 & \cdots \\ \cdots & \mathcal{C}^{-2} & \mathcal{C}^{-1} & \mathcal{C}^0 & \mathcal{C}^1 & \cdots \\ \cdots & \mathcal{C}^{-3} & \mathcal{C}^{-2} & \mathcal{C}^{-1} & \mathcal{C}^0 & \cdots \\ \iddots & \vdots & \vdots & \vdots & \vdots & \ddots \end{pmatrix}, \quad \mathfrak{u} = \begin{pmatrix} \vdots \\ \mathbf{u}^{-1} \\ \mathbf{u}^0 \\ \mathbf{u}^1 \\ \mathbf{u}^2 \\ \vdots \end{pmatrix}, \quad \mathfrak{B} = \begin{pmatrix} \ddots & \vdots & \vdots & \vdots & \vdots & \iddots \\ \cdots & \mathcal{B}_{-1} & 0 & 0 & 0 & \cdots \\ \cdots & 0 & \mathcal{B}_0 & 0 & 0 & \cdots \\ \cdots & 0 & 0 & \mathcal{B}_1 & 0 & \cdots \\ \cdots & 0 & 0 & 0 & \mathcal{B}_2 & \cdots \\ \iddots & \vdots & \vdots & \vdots & \vdots & \ddots \end{pmatrix}.$$

Here, $\mathfrak{C}$ is the (block) Laurent operator corresponding to the symbol $\mathcal{C}^\alpha$. With this notation, equation (3.3) reads

$$\mathfrak{B}\mathfrak{C}\mathfrak{u} = \omega_0^2 \mathfrak{u}. \tag{3.6}$$

The equation (3.6) characterizes the subwavelength resonant frequencies and their corresponding resonant modes. A localized mode corresponds to an eigenvalue of the operator $\mathfrak{B}\mathfrak{C}$. In the periodic case (when $\mathfrak{B} = I$), the spectrum of the Laurent operator $\mathfrak{C}$ is continuous and does not contain eigenvalues, so there are no localized modes. The spectral bands are given by Theorem 3.3 in this case. As we shall see, the operator $\mathfrak{B}\mathfrak{C}$ might have a pure-point spectrum in the non-periodic case.

Remark 3.6. This Laurent-operator formulation generalizes the approach used in [7].

3.3 Toeplitz matrix formulation for compact defects

In this section, we assume that the operators B_m are identity for all but finitely many m. For simplicity, we phrase this analysis in the case $\Lambda = \mathbb{Z}$, where we assume that the resonators corresponding to $0 \leq m \leq M$ have differing parameters, *i.e.*,

$$b_i^m = \begin{cases} 1, & m < 0 \text{ or } m > M, \\ 1 + x_i^m, & 0 \leq m \leq M. \end{cases} \tag{3.7}$$

for some parameters x_i^m. We let X_m be the diagonal matrix with entries x_i^m. In this setting, we obtain a (block) Toeplitz matrix formulation. For $\omega \notin \sigma(\mathfrak{C})$, we define

$$\mathcal{T}(\omega) = \begin{pmatrix} T^0 & T^1 & T^2 & \cdots & T^M \\ T^{-1} & T^0 & T^1 & \cdots & T^{M-1} \\ T^{-2} & T^{-1} & T^0 & \cdots & T^{M-2} \\ \vdots & \vdots & \vdots & \ddots & \vdots \\ T^{-M} & T^{-(M-1)} & T^{-(M-2)} & \cdots & T^0 \end{pmatrix}, \qquad T^m = -\frac{1}{|Y^*|} \int_{Y^*} e^{\mathrm{i}\alpha m} \mathcal{C}^\alpha \left(\mathcal{C}^\alpha - \omega^2 I\right)^{-1} \, \mathrm{d}\alpha.$$

Proposition 3.7. *Assume that $\Lambda = \mathbb{Z}$ and that b_i^m are given by (3.7). Then $\omega_0 \notin \sigma(\mathfrak{C})$ is an eigenvalue of (3.6) if and only if*

$$\det\bigl(I - \mathcal{X}\mathcal{T}(\omega_0)\bigr) = 0,$$

where $\mathcal{X}$ is the block-diagonal matrix with entries X_m.

Proof. From (3.5) it follows that, for each m, we have

$$\mathcal{I}\bigl[\mathcal{B}_m \mathcal{C}^\alpha \mathbf{u}^\alpha\bigr](m) = \omega_0^2 \mathcal{I}\bigl[\mathbf{u}^\alpha\bigr](m).$$

Since X_m is only nonzero for $m = 0, 1, ..., M$, we have

$$\mathcal{I}\Bigl[(\mathcal{C}^\alpha - \omega_0^2 I)\mathbf{u}^\alpha + X_m \mathcal{C}^\alpha \mathbf{u}^\alpha\Bigr](m) = 0, \qquad 0 \leq m \leq M, \tag{3.8}$$

$$\mathcal{I}\Bigl[(\mathcal{C}^\alpha - \omega_0^2 I)\mathbf{u}^\alpha\Bigr](m) = 0, \qquad m < 0 \text{ or } m > M. \tag{3.9}$$

In other words, $(\mathcal{C}^\alpha - \omega_0^2 I)\mathbf{u}^\alpha$ is given by a finite Fourier series in α:

$$(\mathcal{C}^\alpha - \omega_0^2 I)\mathbf{u}^\alpha = \sum_{m=0}^{M} \mathbf{c}_m e^{\mathrm{i}\alpha m},$$

where $\mathbf{c}_m = \mathcal{I}[X_m \mathcal{C}^\alpha \mathbf{u}^\alpha](m)$. Together with (3.8) we find that

$$\mathbf{c}_n = -X_n \sum_{m=0}^{M} \frac{1}{|Y^*|} \int_{Y^*} e^{\mathrm{i}\alpha(m-n)} \mathcal{C}^\alpha (\mathcal{C}^\alpha - \omega_0^2 I)^{-1} \mathbf{c}_m \, \mathrm{d}\alpha.$$

If we denote $\mathbf{c} = \begin{pmatrix} \mathbf{c}_0 \\ \vdots \\ \mathbf{c}_M \end{pmatrix}$, we then obtain the following non-linear eigenvalue problem in ω_0,

$$\mathcal{X}\mathcal{T}(\omega_0)\mathbf{c} = \mathbf{c}, \tag{3.10}$$

where $\mathcal{X}$ is the block-diagonal matrix with entries X_m. □

Remark 3.8. The localized modes can, equivalently, be described by the Toeplitz matrix with entries

$$\widetilde{T}^m = \frac{1}{|Y^*|}\int_{Y^*} e^{\mathrm{i}\alpha m}\left(\mathcal{C}^\alpha - \omega^2 I\right)^{-1}\,\mathrm{d}\alpha,$$

leading to the non-linear eigenvalue problem

$$\omega^2 \mathcal{Y}\widetilde{\mathcal{T}}(\omega_0)\mathbf{c} = \mathbf{c},$$

where $\mathcal{Y} = (I+\mathcal{X})^{-1} - I$.

Remark 3.9. The analysis in this section generalizes approaches found in [3] and [6, 8].

4 Finite perturbations of a chain

In this section, we take the specific example of a chain of equidistant resonators where a finite number of resonators are perturbed, as illustrated in Figures 2(a) and (b). Specifically, we have the lattice dimension $d_l = 1$, the space dimension $d = 3$ and we take a unit cell with just a single resonator: $N = 1$. As we shall see, a single defect may induce a one localized mode. When multiple defects hybridize, level repulsion will guarantee the existence of at least one localized mode. We emphasize that the phenomena highlighted in this section are not specific to the dimensionality and will be qualitatively similar in $d_l = 2$ or $d_l = 3$; see, for example, Figure 1.

4.1 Single defect

We assume that $N = 1$ and that the resonator corresponding to $m = 0$ has a different parameter, *i.e.*,

$$b_1^m = \begin{cases} 1, & m \neq 0, \\ 1+x, & m = 0, \end{cases} \tag{4.1}$$

for some parameter $x > -1$. In the single-resonator case, $\mathcal{C}^\alpha$ is just a scalar $\mathcal{C}^\alpha = \omega_1^\alpha$. It follows from Proposition 3.7 that any eigenvalue ω satisfies $xT^0(\omega) = 1$; in other words that

$$\frac{x}{|Y^*|}\int_{Y^*} \frac{\omega_1^2}{\omega^2 - \omega_1^2}\,\mathrm{d}\alpha = 1. \tag{4.2}$$

For $\omega > \max_{\alpha\in Y^*}\omega_1^\alpha$, it is clear that $T^0(\omega) > 0$. Therefore, there are no solutions in the case $x \leq 0$. Moreover,

$$\lim_{\omega \to \max\limits_{\alpha\in Y^*}\omega_1^\alpha} T^0(\omega) = \infty, \qquad \lim_{\omega\to\infty} T^0(\omega) = 0.$$

Therefore, if $x > 0$, there is a solution $\omega = \omega_*$ of (4.2). In other words, the defect induces an eigenvalue ω_*^2 in the pure-point spectrum of $\mathfrak{BC}$, corresponding to an exponentially localized eigenmode.

The expected localized eigenmode is shown in Figure 3(a) for a finite system of 31 circular resonators. Here, the capacitance matrix was numerically computed using the multipole expansion method (see, *e.g.* the appendix of [4]).

4.2 Double defect

Next, we continue with the case $N = 1$ but now assume that there are two defects at the resonators corresponding to $m = 0$ and $m = M$;

$$b_1^m = 1,\ m \notin \{0, M\}, \qquad b_1^0 = 1 + x_1, \qquad b_1^M = 1 + x_2, \tag{4.3}$$

for some parameters $x_1, x_2 \neq 0$. In this case, the localized modes are characterized by the Topelitz matrix formulation

$$\mathcal{X}\mathcal{T}(\omega)\mathbf{c} = \mathbf{c},$$

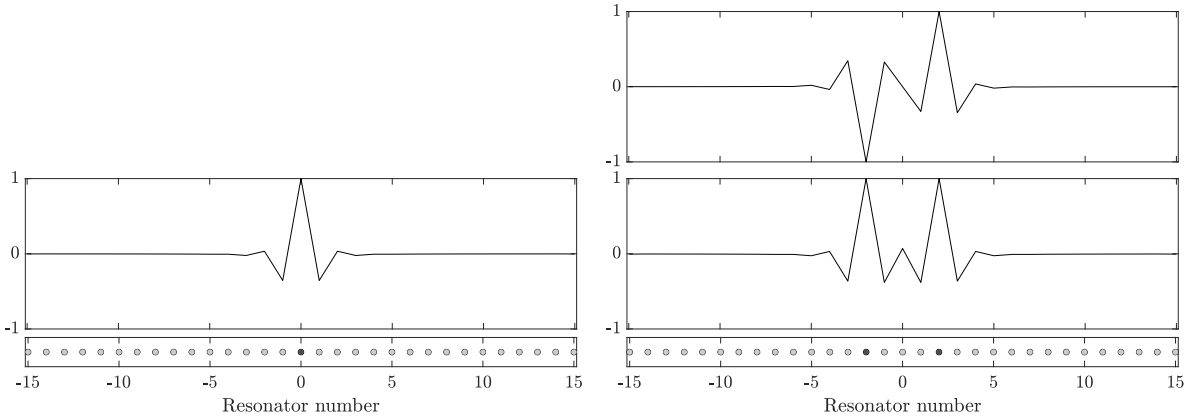

(a) (b)

Figure 3: (a) Plot of the localized mode along the x_1-axis in the case of a single defect with $x = 0.15$. A sketch of the resonator structure is shown below: here we have a chain of $N = 31$ equally spaced circular resonators with the perturbation $1 \mapsto 1 + x$ made to the material parameters of centre resonator. We observe a single localized mode even in the case of small $x > 0$, with larger x leading to a stronger degree of localization (a faster decaying mode). However, in the case $-1 < x < 0$ there are no localized modes. (b) The two localized modes that exist when two defects are introduced with perturbation strengths $x_1 = x_2 = 0.15$ and separation distance $M = 4$. In this case, the higher mode has a dipole (odd) symmetry whole the lower mode has a monopole (even) symmetry.

where

$$\mathcal{X} = \begin{pmatrix} x_1 & 0 & 0 & \cdots & 0 \\ 0 & 0 & 0 & \cdots & 0 \\ 0 & 0 & 0 & \cdots & 0 \\ \vdots & \vdots & \vdots & \ddots & \vdots \\ 0 & 0 & 0 & \cdots & x_2 \end{pmatrix}, \quad \mathcal{T}(\omega) = \begin{pmatrix} T^0 & T^1 & T^2 & \cdots & T^M \\ T^{-1} & T^0 & T^1 & \cdots & T^{M-1} \\ T^{-2} & T^{-1} & T^0 & \cdots & T^{M-2} \\ \vdots & \vdots & \vdots & \ddots & \vdots \\ T^{-M} & T^{-(M-1)} & T^{-(M-2)} & \cdots & T^0 \end{pmatrix}, \quad T^m = -\frac{1}{|Y^*|} \int_{Y^*} \frac{\omega_1^2 e^{\mathrm{i}\alpha m}}{\omega_1^2 - \omega^2} \, \mathrm{d}\alpha.$$

In other words, we are solving the equation

$$\det(I - \mathcal{X}\mathcal{T}(\omega)) = 0.$$

We observe that

$$\det(I - \mathcal{X}\mathcal{T}(\omega)) = \det\left(I - \begin{pmatrix} x_1 T^0 & x_1 T^M \\ x_2 T^{-M} & x_2 T^0 \end{pmatrix}\right),$$

so we seek the solutions ω to

$$\big(1 - x_1 T^0(\omega)\big)\big(1 - x_2 T^0(\omega)\big) - x_1 x_2 T^{-M}(\omega) T^M(\omega) = 0. \tag{4.4}$$

In Figure 4 we show the resonant frequencies of defect modes in a system with two defects. These are obtained by solving (4.4) for $x_1 = x_2 = x$ and varying either x or the separation distance M. We see that for any $x > 0$ there is at least one localized eigenmode. If either M or x is small, then there is only one solution, as the hybridization means the smaller solution is not greater than the maximum of the Bloch band so there is no localized eigenmode. For any fixed x there is a critical minimum value M_{sep} of M in order for two localized eigenmodes to exist. In Figure 4(c) we show the relation between the critical values for the distance M and the perturbation strength x.

4.2.1 Level repulsion in a two-defect structure

In Figure 5 we model the resonant frequencies of a system with two random defects. In particular, we assume that the values of x_1 and x_2 are drawn independently from the uniform distribution $U[\mu - \sqrt{3}\sigma, \mu + \sqrt{3}\sigma]$. We see that for small σ there are still two localized modes, however for larger values of σ the eigenfrequencies can be be lost into the spectral band. Nevertheless, looking at Figure 5b we see that the introduction of random perturbations causes the average value of each mid-gap frequency to move further apart (and further from the edge of the band gap). This is the phenomenon of level repulsion. One consequence of this is that the eigenmodes, on average, become more strongly localized

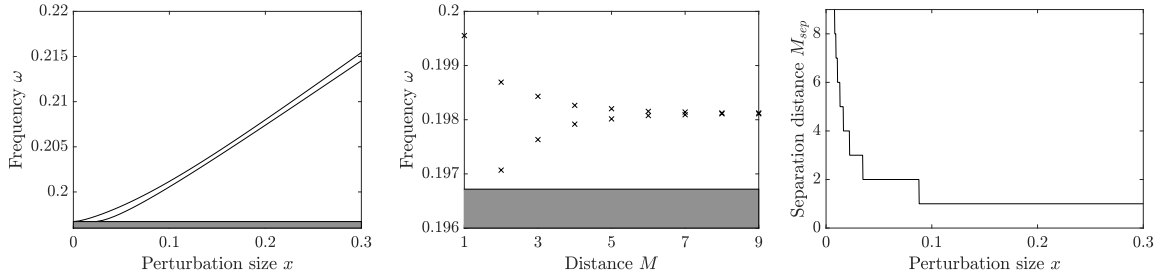

(a) *(b)* *(c)*

Figure 4: Localized frequencies for two defects, for the case of identical defects $x_1 = x_2 = x$. (a) Solutions ω of (4.4) as function of the perturbation size x for fixed distance $M = 3$. (b) Solutions ω of (4.4) as function of the distance M for fixed perturbation size $x = 0.05$. If either M or x is small, then there is only one solution, as the level repulsion causes the second solution to fall within the spectral band (denoted by the shaded area). (c) The minimum separation distance M_{sep} required to obtain two solutions to (4.4), plotted as a function of x in the case $x_1 = x_2 = x$.

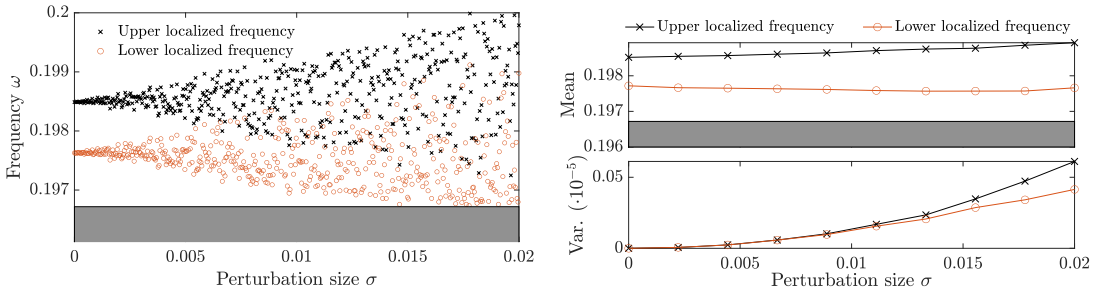

(a) *(b)*

Figure 5: Localized frequencies for two random defects. (a) Solutions ω of (4.4) with x_1 and x_2 drawn from a uniform $U[\mu - \sqrt{3}\sigma, \mu + \sqrt{3}\sigma]$ distribution, with varying σ, fixed mean $\mu = 0.05$ and fixed separation distance $M = 6$. (b) The mean (upper) and variance (lower) of the localized frequencies ω for different values of σ, fixed mean $\mu = 0.05$ and fixed $M = 3$. For each simulated value of σ, 1000 simulated values are used to compute the mean and variance, with values being left empty when no such frequency exists (e.g. when there is only one solution to (4.4), as the hybridization causes the second solution to fall within the spectral band).

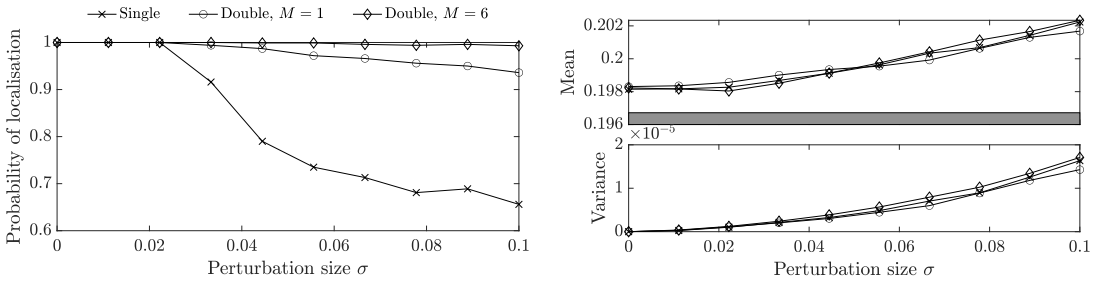

(a) *(b)*

Figure 6: Comparison of the robustness of systems with one or two defects. (a) The probability of at least one localized mode existing for the case of a single defect, a double defect with separation distance $M = 1$ and a double defect with separation distance $M = 6$. In each case, the perturbations are drawn at random from a uniform distribution $U[\mu - \sqrt{3}\sigma, \mu + \sqrt{3}\sigma]$ and, for very large values of σ we enforce $1 + x_i \geq 10^{-4} > 0$, so that the material parameters are all strictly positive. The means are chosen as $\mu = 0.05$, $\mu = 0.0325$ and $\mu = 0.05$, respectively, so that the largest localized eigenfrequency is the same in each case when $\sigma = 0$. (b) The mean and variance of the largest localized eigenfrequency for the three different models. Each value was calculated using 1000 independent random realisations.

as the variance σ^2 increases (since the strength of the localization increases when the resonant frequency is further from the edge of the band gap).

Another consequence of level repulsion is that the existence of localized modes is much more robust in the case of two defects than in the case of a single defect. Figure 6(a) shows the probability of at least one localized eigenmode existing for three different cases: a single defect, a double defect with small separation distance $M = 1$ and a double defect with larger separation distance $M = 6$. The defects are normally distributed with means chosen to normalize the distributions in the sense that the largest defect frequency when $\sigma = 0$ is the same in all three cases ($\omega = 0.198$). We see that the probability of localization drops off quickly for a single defect. When $\sigma = 0.1$, the probability of localization for a single defect is 65.6%, compared to 93.6% for the double defect with small separation distance and 99.3% when the separation distance is larger. The intuitive explanation for the difference between the two double defect cases is that the larger distance causes the two localized eigenfrequencies to be closer together in the deterministic case of $\sigma = 0$, meaning that they interact with one another more strongly so the level repulsion has a greater effect. When at least one localized eigenmode exists, the distributions of the largest localized eigenvalue, shown in Figure 6(b), are similar in all three cases.

4.2.2 Phase transition and eigenmode symmetry swapping

Analogously to Figure 4(a), Figure 7(a) shows the two localized frequencies, but here in the case $M = 2$. When M is even, the two curves will intersect (here around $x \approx 0.2$), corresponding to a doubly degenerate frequency. Crucially, this is a transition point whereby the symmetries of the corresponding eigenmodes swap. Below the transition point, the first mode has dipole (odd) symmetry while the second mode has monopole (even) symmetry; above the transition point the first mode has monopole symmetry while the second mode has dipole symmetry.

Next, we study the degree of localization around this transition point. Throughout, we define the degree of localization $l(u)$ of an eigenmode u as

$$l(u) = \frac{\|u\|_\infty}{\|u\|_2}. \tag{4.5}$$

We remark that $0 < l(u) \leq 1$: small $l(u)$ corresponds to a delocalized mode while $l(u) = 1$ corresponds to a mode which is perfectly localized to a single resonator.

In Figure 7(b) we plot the average degree of localization when the parameters are drawn independently from $\mathcal{U}[x - \sqrt{3}\sigma, x + \sqrt{3}\sigma]$ for $\sigma = 10^{-4}$. The plot shows a sharp peak at the transition point; a remarkably high degree of localization is achieved even when the variance is small. This can be understood as a decoupling of the (otherwise coupled) modes, which, at the transition point, become concentrated to the individual defects as opposed to both defects.

For higher values of σ, we expect to achieve a strong degree of localization for a larger range of x. As seen in Figure 7(c), there is a region in the x-σ-plane where we achieve optimal localization. When x is large relative to σ, the modes will couple and the degree of localization is low. When σ is large relative to x, we are in a regime with, on average, only a single localized mode.

4.3 Many defects

The motivation for the above analyses of systems with one or two local defects is to be able to infer properties of fully random systems, which will be studied in Section 5. To further this analysis, we again assume that $N = 1$ and consider a system with N_d independent defects. That is, we assume that

$$b_1^m = 1,\ m \notin \{0, M, 2M, \ldots, N_d M\} \quad \text{and} \quad b_1^{kM} = 1 + x_k,\ k \in \{0, 1, 2, \ldots, N_d\}, \tag{4.6}$$

for some parameters $x_1, \ldots, x_{N_d} \neq 0$. In this case, we can use the Topelitz matrix formulation from before to see that the localized modes are characterized by the equation

$$\det\left(I - \mathcal{A}_{\mathcal{XT}}(\omega)\right) = 0, \tag{4.7}$$

where $\mathcal{A}_{\mathcal{XT}}(\omega)$ is the $N_d \times N_d$ matrix given by

$$\mathcal{A}_{\mathcal{XT}}(\omega)_{ij} = x_i T^{M(j-i)}(\omega) \quad \text{with} \quad T^m = -\frac{1}{|Y^*|}\int_{Y^*} \frac{\omega_1^2 e^{\mathrm{i}\alpha m}}{\omega_1^2 - \omega^2}\,\mathrm{d}\alpha.$$

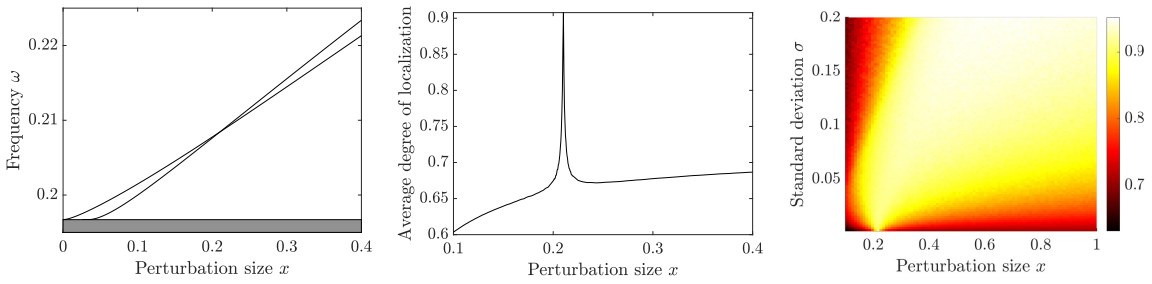

(a) *(b)* *(c)*

Figure 7: Localized frequencies for two defects, for the case of $M = 2$. (a) Solutions ω of (4.4), in the case of identical defects $x_1 = x_2 = x$, as function of the perturbation size x. The two curves intersect around $x \approx 0.21$. (b) Localization length $l(u)$ of the two modes, with parameters drawn independently from $\mathcal{U}[x - \sqrt{3}\sigma, x + \sqrt{3}\sigma]$ for $\sigma = 10^{-4}$. At the intersection, the monopole/dipole modes decouple, resulting in a sharp peak of $l(u)$. (c) Average degree of localization for different x and σ. The peak seen in (b) becomes wider for larger σ, giving rise to a region in the x-σ-plane with high degree of localization.

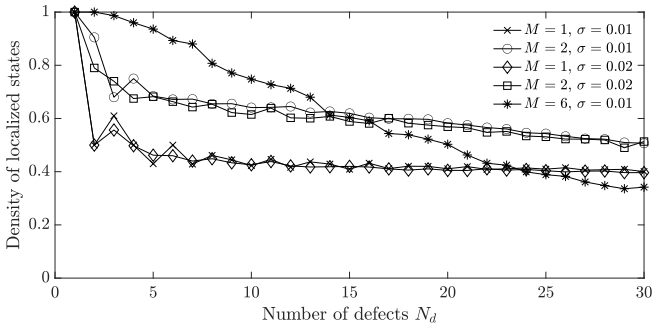

Figure 8: Localized modes for increasingly many defects. We plot the average number of localized modes divided by the number of defects for increasing numbers of defects. The defects are drawn from a uniform $U[0.05 - \sqrt{3}\sigma, 0.05 + \sqrt{3}\sigma]$ distribution and have separation distance M. Each point is an average over 100 independent random realisations.

We can solve the system (4.7) to find the localized modes for a system of N_d defects. In Figure 8 we show how the number of localized modes varies as the number of defects N_d increases. The number of localized modes is normalized by dividing by the number of defects N_d, to give a measure of the density of localized modes (the number of defects is proportional to the length of the part of the resonator chain that contains the defects, which has length $N_d M$). Different values of M and σ are compared. In all cases, we observe that as N_d becomes large the system appears to converge to a state whereby between 30% and 50% of the modes are localized.

5 Fully random parameter distribution

We now study the case when all parameters b_i^m are randomly distributed. We assume that

$$b_i^m = 1 + \sigma X_i^m, \qquad \mathfrak{B} = I + \sigma \mathfrak{X},$$

where $\mathfrak{X}$ is a diagonal operator. Here, we take X_i^m to be independent and uniformly distributed on $[-\sqrt{3}, \sqrt{3}]$. In order to guarantee that the material parameters remain positive, we require $\sigma < \frac{1}{\sqrt{3}}$.

Localized modes are characterized by the equation

$$(\mathfrak{C} + \sigma \mathfrak{X} \mathfrak{C})\, \mathfrak{u} = \omega^2 \mathfrak{u}. \tag{5.1}$$

In other words, we have characterized the problem in terms of the spectral problem for a random perturbation of a discrete operator. We emphasize that the unperturbed part of the operator, namely $\mathfrak{C}$, is a dense matrix, whose off-diagonal terms describe long-range interactions with slow decay like

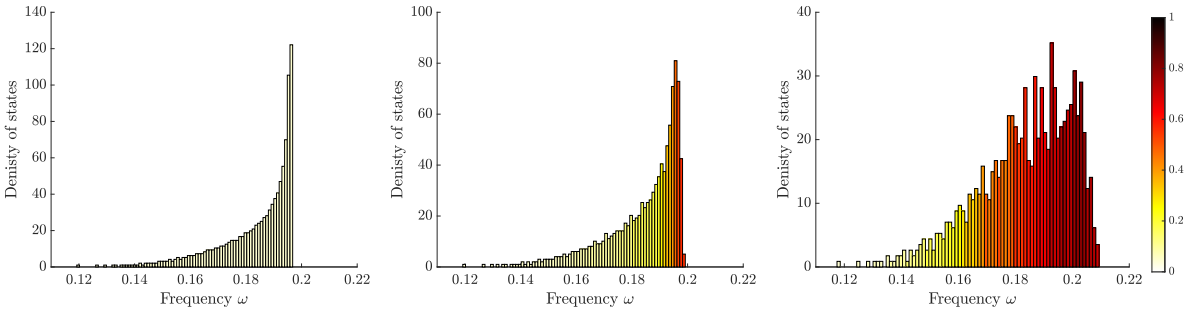

(a) $\sigma = 0$ *(b)* $\sigma = 0.02$. *(c)* $\sigma = 0.1$.

Figure 9: Example outcome of the density of states in a chain of equally spaced resonators with uniformly distributed random parameters. Additionally, the colour shows the average degree of localization $l(u) = \|u\|_\infty / \|u\|_2$*, where large* $l(u)$ *corresponds to a strongly localized mode* u*. In this case, there is a single spectral band, between* 0 *and* ~ 0.2*, when* $\sigma = 0$*. For small but nonzero* σ*, localized modes emerge at the edge of this band, while a bigger part. Here shown for a finite chain of* $N = 1000$ *resonators.*

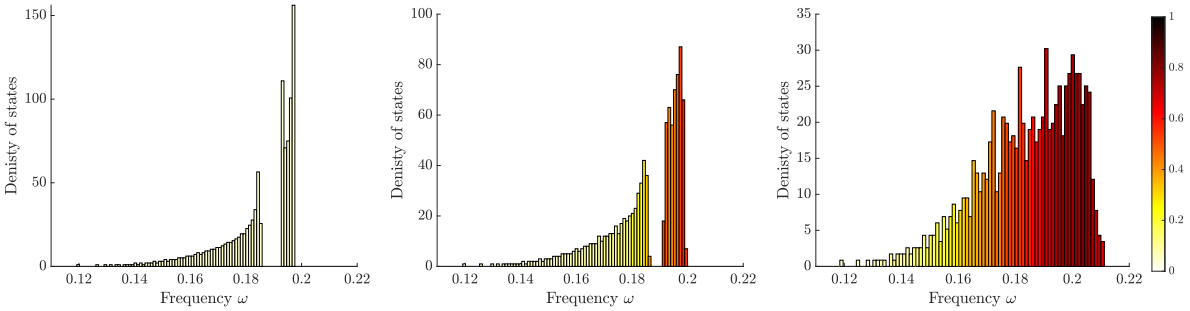

(a) $\sigma = 0$ *(b)* $\sigma = 0.02$. *(c)* $\sigma = 0.1$.

Figure 10: Example outcome of the density of states in a chain of resonator dimers with uniformly distributed random parameters. Additionally, the colour shows the (normalized) average degree of localization $l(u) = \|u\|_\infty / \|u\|_2$*, where large* $l(u)$ *corresponds to a strongly localized mode* u*. The case* $\sigma = 0$ *exhibits two spectral bands, separated by a band gap. For small but nonzero* σ*, localized modes emerge around the edges of the bands: above the first band, and below and above the second band. When* σ *increases, the band gap vanishes and the density of localized modes increases across the spectrum. Here shown for a finite chain of* $N = 1000$ *resonators.*

$1/|i-j|$. Additionally, the perturbation $\sigma\mathfrak{X}\mathfrak{C}$ is also a dense matrix, containing random perturbations to both the diagonal- and off-diagonal terms. These two properties make the problem considerably more challenging than Anderson's original model, and precise statements on the spectrum of $\mathfrak{C} + \sigma\mathfrak{X}\mathfrak{C}$ are generally beyond reach.

5.1 Band structure and emergence of localized modes

In Figure 9, we show the numerically computed density of states, along with the average degree of localization. Here, we take a chain of equally spaced resonators, which in the case $\sigma = 0$ has a single spectral band. Localized modes emerge as σ becomes nonzero, whose frequencies lie around the edge of the spectral band. Increasing σ leads to more localized modes and a stronger degree of localization.

Next, we turn to the case $N = 2$. Here, we take a chain of "dimers", *i.e.* a chain of resonators with alternating, unequal, separation distance, as depicted in Figure 2(d). In the case $\sigma = 0$, which was studied extensively in [4], we have two spectral bands separated by a band gap. For small but nonzero σ, the band gap persists and localized modes emerge at either edge of the bands. Increasing σ further, more modes become localized and the band-gap structure disappears.

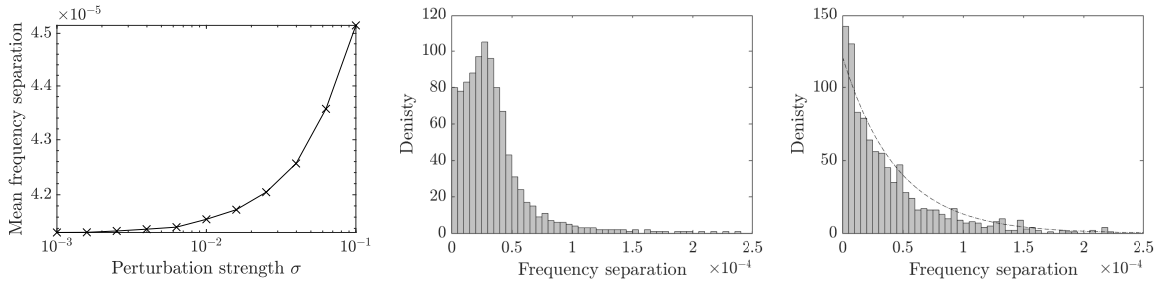

(a) *(b)* $\sigma = 0.001$ *(c)* $\sigma = 0.1$

Figure 11: Level repulsion in a finite chain of $N = 1000$ resonators with random perturbations. (a) The average nearest-neighbour separation between the (real parts of the) resonant frequencies for different perturbation strengths σ, which is the standard deviation of the uniform random variables. (b) and (c) are histograms showing the distributions of the normalized frequency separations (frequency separation divided by mean frequency separation) for $\sigma = 10^{-3}$ and $\sigma = 10^{-1}$, respectively. A distribution of the form $\exp(-x)$ is shown with a dashed line on (c), for comparison.

5.2 Level repulsion in the fully random case

Many of the arguments presented in this work involve the principle of level repulsion: that eigenvalues would tend to separate when increasingly large random errors are added. This was demonstrated in the double defect case in Figure 5(b). We can also study the level repulsion in a finite chain of equally spaced resonators. In particular, Figure 11(a) shows that the average separation increases as the perturbation strength σ increases. We also show the distributions of the separations for two specific values of σ in Figures 11(b) and 11(c). In Figure 11(b), the perturbations are so small that this distribution is (visually) the same as that of the unperturbed structure. In Figure 11(c), the larger perturbations have affected the shape of the distribution. A distribution of the form $\exp(-x)$ is shown, for comparison, which is also seen in other randomly perturbed spectral problems (see *e.g.* Figures 2 and 3 of [11]). It is worth noting that much of the standard theory of eigenvalues of random matrices is not useful in this case. First, we are making a very specific choice of unperturbed structure, which is periodic and has spectral structure (which is the main factor determining the distribution in Figure 11(b)). Additionally, the random perturbations are encoded in the diagonal matrix $\mathfrak{X}$, such that the entries of $\mathfrak{C} + \sigma\mathfrak{X}\mathfrak{C}$ are not independent from one another (entries in the same row have non-zero covariance).

6 Conclusions

Using the generalized capacitance formulation, we have described Anderson localization in systems of high-contrast subwavelength resonators. Starting from first principles, we derived a discrete asymptotic approximation of the resonant states of the high-contrast Helmholtz problem. This takes the form of a Laurent operator with long-range off-diagonal terms and a multiplicative perturbation factor. This can be solved explicitly in the case of compact defects, yielding exact formulas which reveal the fundamental mechanisms of subwavelength localization and explain the phenomena observed in random systems. Specifically, we characterized the localization in terms of level repulsion, which causes the eigenfrequencies to spread and corresponding modes to become localized. Additionally, we were able to identify a phase transition as an eigenmode swapping event and show that, at this phase transition, strong localization is achievable with an exceptionally small random perturbation. Finally, we studied fully random systems, where localized modes emerge around any edge of the band functions of the unperturbed structure and have properties that can be understood using our earlier results on compact defects.

Acknowledgements

The work of HA was partly funded by the Swiss National Science Foundation grant number 200021–200307. The work of BD was partly funded by the EC-H2020 FETOpen project BOHEME under grant

agreement 863179. The code used in this study is available at `https://doi.org/10.5281/zenodo.6577767`.

References

[1] M. Aizenman and S. Molchanov. Localization at large disorder and at extreme energies: An elementary derivations. *Commun. Math. Phys.*, 157(2):245–278, 1993.

[2] H. Ammari, B. Davies, and E. O. Hiltunen. Functional analytic methods for discrete approximations of subwavelength resonator systems. *arXiv preprint arXiv:2106.12301*, 2021.

[3] H. Ammari, B. Davies, and E. O. Hiltunen. Robust edge modes in dislocated systems of subwavelength resonators. *To appear in J. London Math. Soc.*, doi:10.1112/jlms.12619, 2022.

[4] H. Ammari, B. Davies, E. O. Hiltunen, and S. Yu. Topologically protected edge modes in one-dimensional chains of subwavelength resonators. *J. Math. Pure. Appl.*, 144:17–49, 2020.

[5] H. Ammari, F. Fiorani, and E. O. Hiltunen. On the validity of the tight-binding method for describing systems of subwavelength resonators. *To appear in SIAM J. Appl. Math.*, 2022.

[6] H. Ammari, B. Fitzpatrick, E. O. Hiltunen, and S. Yu. Subwavelength localized modes for acoustic waves in bubbly crystals with a defect. *SIAM J. Appl. Math.*, 78(6):3316–3335, 2018.

[7] H. Ammari and E. O. Hiltunen. Edge modes in active systems of subwavelength resonators. *arXiv preprint arXiv:2006.05719*, 2020.

[8] H. Ammari, E. O. Hiltunen, and S. Yu. Subwavelength guided modes for acoustic waves in bubbly crystals with a line defect. *J. Eur. Math. Soc.*, 24(7):2279–2313, 2022.

[9] P. W. Anderson. Absence of diffusion in certain random lattices. *Phys. Rev.*, 109(5):1492, 1958.

[10] J. Billy, V. Josse, Z. Zuo, A. Bernard, B. Hambrecht, P. Lugan, D. Clément, L. Sanchez-Palencia, P. Bouyer, and A. Aspect. Direct observation of Anderson localization of matter waves in a controlled disorder. *Nature*, 453(7197):891–894, 2008.

[11] T. A. Brody, J. Flores, J. B. French, P. A. Mello, A. Pandey, and S. S. M. Wong. Random-matrix physics: spectrum and strength fluctuations. *Rev. Mod. Phys.*, 53(3):385, 1981.

[12] R. Carmona. Exponential localization in one dimensional disordered systems. *Duke Math. J.*, 49(1):191–213, 1982.

[13] T. Crane, O. J. Trojak, J. P. Vasco, S. Hughes, and L. Sapienza. Anderson localization of visible light on a nanophotonic chip. *ACS Photonics*, 4(9):2274–2280, 2017.

[14] A. Figotin and A. Klein. Localization of electromagnetic and acoustic waves in random media. lattice models. *J. Stat. Phys.*, 76(3):985–1003, 1994.

[15] M. Filoche and S. Mayboroda. Universal mechanism for Anderson and weak localization. *Proc. Natl. Acad. Sci. USA*, 109(37):14761–14766, 2012.

[16] J.-P. Fouque, J. Garnier, G. Papanicolaou, and K. Solna. *Wave propagation and time reversal in randomly layered media*, volume 56 of *Stochastic Modelling and Applied Probability*. Springer Science & Business Media, 2007.

[17] J. Fröhlich, F. Martinelli, E. Scoppola, and T. Spencer. Constructive proof of localization in the Anderson tight binding model. *Commun. Math. Phys.*, 101(1):21–46, 1985.

[18] J. Fröhlich and T. Spencer. Absence of diffusion in the Anderson tight binding model for large disorder or low energy. *Commun. Math. Phys.*, 88(2):151–184, 1983.

[19] H. Herzig Sheinfux, I. Kaminer, A. Z. Genack, and M. Segev. Interplay between evanescence and disorder in deep subwavelength photonic structures. *Nat. Commun.*, 7(1):1–9, 2016.

[20] A. Ishimaru. *Wave propagation and scattering in random media*. Academic Press New York, 1978.

[21] S. D. Jenkins, N. Papasimakis, S. Savo, N. I. Zheludev, and J. Ruostekoski. Strong interactions and subradiance in disordered metamaterials. *Phys. Rev. B*, 98(24):245136, 2018.

[22] A. Lagendijk, B. Van Tiggelen, and D. S. Wiersma. Fifty years of Anderson localization. *Phys. Today*, 62(8):24–29, 2009.

[23] M. L. Mehta. *Random Matrices and the Statistical Theory of Energy Levels*. Academic Press, Boston, 1967.

[24] M. Minnaert. On musical air-bubbles and the sounds of running water. *Philos. Mag.*, 16(104):235–248, 1933.

[25] R. M. Nandkishore and S. L. Sondhi. Many-body localization with long-range interactions. *Phys. Rev. X*, 7(4):041021, 2017.

[26] M. Segev, Y. Silberberg, and D. N. Christodoulides. Anderson localization of light. *Nat. Photonics*, 7(3):197–204, 2013.

[27] H. H. Sheinfux, Y. Lumer, G. Ankonina, A. Z. Genack, G. Bartal, and M. Segev. Observation of Anderson localization in disordered nanophotonic structures. *Science*, 356(6341):953–956, 2017.

[28] E. J. Torres-Herrera, J. Méndez-Bermúdez, and L. F. Santos. Level repulsion and dynamics in the finite one-dimensional Anderson model. *Phys. Rev. E*, 100(2):022142, 2019.